Check for updates

Neutral nickel complexes with tetradentate N-heterocyclic carbene amidate ligands for electrocatalytic hydrogen evolution†

Si Si,[a] Wenxun Song,[a] Jie Chen,*[a] Weimin Zhang,[a] Wenhua Ji, [ID][c] Wonwoo Nam [ID] *[b] and Bin Wang [ID] *[a]

Neutral nickel complexes bearing tetradentate N-heterocyclic carbene (NHC) amidate ligands were prepared; the effect of the electronic properties of the ligand on the redox behavior as well as the electrocatalytic activity for hydrogen evolution reaction (HER) were investigated.

Hydrogen (H_2) is a clean energy source that only produces water vapor when combusted.[1] It can be produced through proton reduction in electrolyzed water under a renewable energy supply. Therefore, electrocatalytic proton reduction is a promising method for producing clean and sustainable fuel. In nature, hydrogenases such as [NiFe], [FeFe], and [Fe] hydrogenases are effective catalysts for HER at ambient temperature and pressure.[2] Inspired by the structural features and catalytic principles of hydrogenases, earth-abundant metal complexes have been synthesized to mimic the HER behaviour of hydrogenases and understand the mechanisms of the HER process.[2] While heterogeneous catalysts like alloys,[3] nanomaterials,[4] and metal–organic frameworks (MOFs)[5] have been studied for their stability and ease of fixation on electrodes for HER, molecular metal complexes are preferred for exploring structure–function relationships, controlling the redox properties, and elucidating HER mechanisms.[6]

Nickel, a non-noble metal from group VIII, is often chosen as a suitable alternative to palladium or platinum in the creation of molecular catalysts due to its readily available oxidation states (including Ni^0, Ni^I, Ni^{II}, Ni^{III}, and Ni^{IV}).[7] In nickel-catalyzed HER, the reduction of Ni(II) to Ni(I) represents

a critical step.[8] Through intelligent ligand design, Ni(II) centers can be coordinated in a way that confers specific catalytic properties to nickel complexes, leveraging their diverse redox abilities.[9] Moreover, nickel serves as the active center in [NiFe] hydrogenase, which plays a crucial role in the reversible conversion of hydrogen and protons.[2] These findings have inspired researchers to develop molecular catalysts based on nickel complexes.[6]

The utilization of N-heterocyclic carbenes (NHCs) in organometallic and coordination chemistry has experienced a resurgence since the isolation of the first stable NHC.[10] NHCs establish stronger bonds with transition metal centers compared to their tertiary phosphine counterparts, owing to their robust σ-donating properties.[10] This enhanced bonding leads to increased stability of the complexes and decreased susceptibility to decomposition from ligand dissociation. Moreover, deprotonated amide or amidate ligands possess increased electron density on the nitrogen atom, which can lead to strong metal–ligand interactions and thus more stable complexes.[11] Therefore, the combination of NHCs with amidates would provide chemically robust complexes, with resistance to oxidation and hydrolysis, making them suitable for a wide range of catalytic transformations.[12,13] In particular, NHC-based nickel complexes have been demonstrated to be good catalysts in electrocatalytic proton reduction yet with high overpotentials (0.86–1.33 V).[12c,d] Furthermore, transition-metal complexes bearing C_2 symmetric tetradentate NHC-amidate ligands have rarely been explored in electrocatalysis.

Herein, we prepare three nickel complexes bearing C_2 symmetric tetradentate NHC-amidate ligands to investigate the effects of the electronic properties of the ligand on the redox behavior as well as the electrocatalytic activity for proton reduction. The electrochemical trends of these complexes shed light on the impact of electronic effect on their electrocatalytic HER activity. Based on the cyclic voltammetry data, an ECEC mechanism (where E represents an electrochemical step and C represents a chemical step) was proposed for the HER in the presence of trifluoroacetic acid (TFA).

[a]*School of Chemistry and Chemical Engineering, University of Jinan, Jinan 250022, Shandong Province, China. E-mail: chm_chenj@ujn.edu.cn, chm_wangb@ujn.edu.cn*
[b]*Department of Chemistry and Nano Science, Ewha Womans University, Seoul 03760, Korea. E-mail: wwnam@ewha.ac.kr*
[c]*Key Laboratory for Applied Technology of Sophisticated Analytical Instruments of Shandong Province, Shandong Analysis and Test Center, Qilu University of Technology (Shandong Academy of Sciences), Jinan 250014, China*

The nickel(II) complexes **1–3** used in this study were synthesized by heating equimolar amounts of anhydrous NiCl$_2$ and the corresponding tetradentate NHC-amidate ligand in anhydrous *N,N*-dimethylformamide (DMF) at 110 °C.[13] Single crystals suitable for X-ray crystallography analysis were obtained by slowly diffusing anhydrous diethyl ether into a DMF solution of complexes **1–3** at room temperature (Fig. 1, see Fig. S1, Tables S1–S3† for the detailed crystal data). All three complexes exhibit C_2 symmetry and are uncharged, with distorted-square-planar coordination geometry attributed to steric repulsion between the methyl groups of the NHC units in **1–3**. The carbene carbon atoms (C1 and C2) are displaced by 0.4723–0.5377 Å above and below the coordination plane defined by Ni1, N1, and N2 (Fig. 1, Table S1†). The geometric parameter (τ_4) has been frequently used as a simple metric to evaluate the geometry of four-coordinate transition metal complexes quantitatively, and it ranges from 0 for ideal square-planar geometry to 1 for ideal tetrahedral geometry.[14] The τ_4 values were determined to be 0.2386 for **1**, 0.2286 for **2**, and 0.2208 for **3** according to eqn (1),[14] where α and β are the two largest L–Ni–L angles (Table S3†).

$$\tau_4 = \frac{360° - (\alpha + \beta)}{141°} \quad (1)$$

These result shows that the τ_4 value of **3** is the smallest, indicating the least distortion in the square plane.

Electrochemical characterization of **1–3** was conducted in anhydrous CH$_3$CN with 0.1 M n-Bu$_4$NPF$_6$ as the supporting electrolyte at a scan rate of 100 mV s^{-1} under N$_2$ atmosphere (Fig. 2). Ferrocene was employed as an internal reference to report potentials relative to Fc/Fc$^+$, and the reported Fc/Fc$^+$ potential values can be converted to *versus* Ag/AgCl by adding
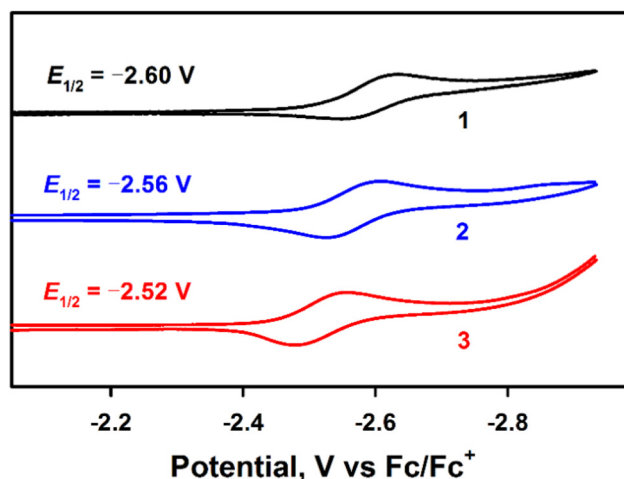
Fig. 2 CVs of 1.0 mM **1** (black line), **2** (blue line), and **3** (red line) in deaerated CH$_3$CN. Conditions: 0.1 M n-Bu$_4$NPF$_6$, GC working electrode, 100 mV s^{-1} scan rate, 25 °C.

0.44 V (Fig. S2†). The cyclic voltammograms (CVs) of **1–3** exhibited a pair of reversible redox features (Fig. 2), indicating a one-electron reaction during the redox process. The Ni^{II}/Ni^{I} redox couples were identified at half-wave potential values of −2.60 V, −2.56 V, and −2.52 V *versus* Fc/Fc$^+$ (Fig. 2), corresponding to **1**, **2**, and **3**, respectively. The shift of redox potentials for Ni^{II}/Ni^{I} to more negative values followed the order **1** > **2** > **3**. The observed shift of the redox potentials to more negative values may be attributed to the increased electron-donating ability of the diamidate group. This enhancement in electron donation strengthens the coordination of the dianionic
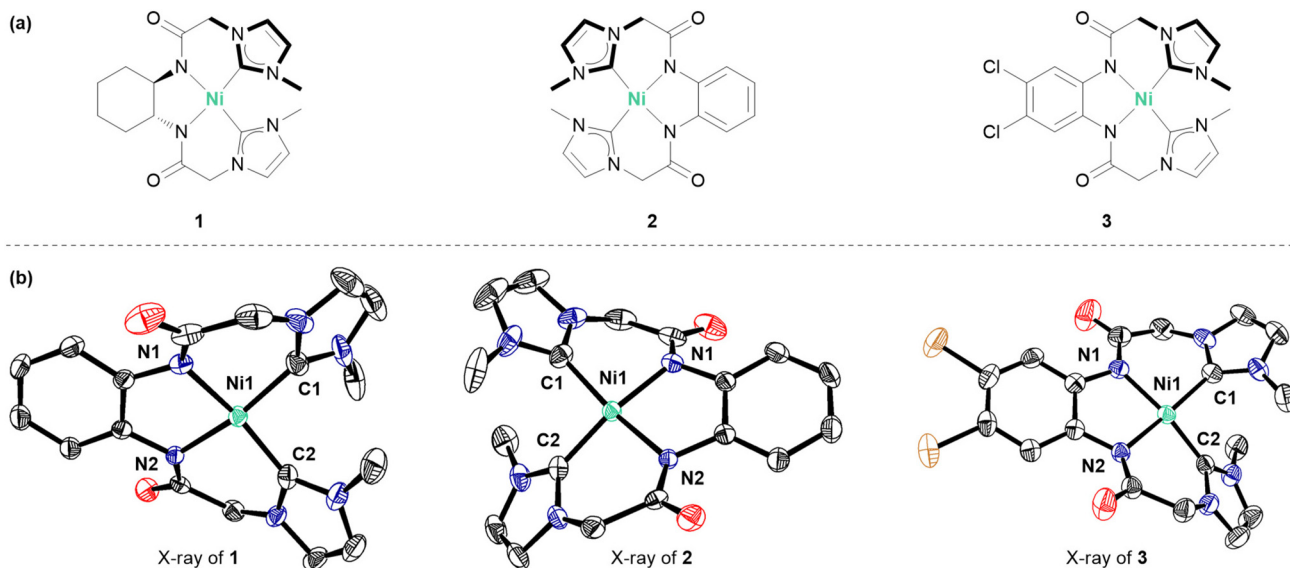
Fig. 1 (a) Molecular structures of nickel complexes **1–3**. (b) X-ray crystal structures of **1–3** as an ORTEP drawing with 50% probability ellipsoids (Ni, medium aquamarine; N, new midnight blue; O, red; Cl, gold; C, black). Selected bond distances (Å) for **1**: Ni–N1 = 1.904(2), Ni–N2 = 1.915(2), Ni–C1 = 1.852(3), Ni–C2 = 1.857(3). For **2**: Ni–N1 = 1.917(2), Ni–N2 = 1.906(2), Ni–C1 = 1.857(3), Ni–C2 = 1.851(3). For **3**: Ni–N1 = 1.904(2), Ni–N2 = 1.908(2), Ni–C1 = 1.849(2), Ni–C2 = 1.848(2).

group to the nickel center, thus leading to more negative redox potentials.[15] The absence of significant peaks associated with the ligand and electrolyte in this region suggests that the electron transfer was not influenced by them (Fig. S3–S5†). The linear correlation between the reduction current (i_p) and the square root of the scan rate indicates that the electrochemical event is diffusion-controlled (Fig. S6†).

The electrochemical hydrogen production capabilities of **1–3** were then investigated in deaerated CH_3CN in the presence of TFA (pK_a = 12.7 in CH_3CN[16]) (Fig. 3). The CVs exhibited significant changes upon addition of TFA (Fig. 3a, c, and e). Control experiments of CVs were also performed in the absence of the nickel(II) complex (Fig. S7†), resulting in lower currents compared to those performed in the presence of the nickel(II) complex. This indicates that the nickel(II) complexes enhance the catalytic activity of HER. To evaluate the electrocatalytic performance of **1–3**, the ratios of catalytic current (i_{cat}) in the presence of TFA to the peak current (i_p) in the absence of TFA were determined (Table 1), and a higher i_{cat}/i_p value signifies a faster catalysis.[15,17] In addition, the catalytic current (i_{cat}) increased linearly with increasing TFA concentration, and the plots of i_{cat} *versus* the concentration of TFA exhibited linear correlations for **1–3** (Fig. 3b, d, and f), as described by eqn (S1).† Moreover, turnover frequency values (TOFs) of 316 s^{-1}, 409 s^{-1}, and 698 s^{-1}, were determined for **1–3**, respectively (Table 1), calculated using the derivation equations (eqn (S2)–(S4)†). Overpotential, which is defined as the disparity between the potential at half-maximum of the catalytic current and the standard potential E°HA of the acid,

Table 1 Bulk electrolysis of **1–3** for electrocatalytic H_2 production[a]

Cat.	τ_4	$E_{1/2}$ (V)	Overpotential (mV)	i_{cat}/i_p	TOF (s^{-1})
1	0.2386	−2.60	780	40	316
2	0.2286	−2.56	770	46	409
3	0.2208	−2.52	760	60	698

[a] These values were obtained from the CVs of **1–3** in deaerated CH_3CN containing 0.1 M n-Bu$_4$NPF$_6$ with a GC working electrode at 25 °C, potentials are *versus* Fc/Fc$^+$, scan rate = 100 mV s^{-1}, [TFA] = 200 mM.

is a crucial parameter for evaluating the electrocatalytic efficiency of a catalyst.[18] The overpotentials for hydrogen generation by **1–3**, estimated using the Evans method (eqn (S5) and (S6)†), were 780 mV for **1**, 770 mV for **2**, and 760 mV for **3** in the presence of TFA (Table 1). It's noteworthy that the electrocatalytic HER performance of **3** ranks in the upper-middle level among the reported molecular nickel catalysts when considering their applied overpotential values (Table S4†). Therefore, the TOFs for electrocatalytic hydrogen production exhibit a significant increase in the order **1** < **2** < **3** (Table 1), and the overpotentials also shift to the positive range in the same order (Table 1). This trend aligns with the reduction potentials of **1–3** (Table 1), indicating that complex **3**, with the most positive potential (Table 1), demonstrates the highest catalytic activity among the three complexes.

To determine the Faraday efficiency (FE) for H_2 production mediated by **1–3**, controlled potential electrolysis (CPE) experiments were conducted at −1.60 V for 3 h (Fig. 4). The amount of H_2 produced was quantified using gas chromatography (GC) at the end of electrolysis (Fig. S8†). The FE values were calculated to be 64% for **3**, 54% for **2**, and 45% for **1** using eqn (S7),† complex **3** exhibited the highest FE and the highest charge passed. Additionally, all complexes showed a linear increase in charge over the 3-hour consecutive electrolysis (Fig. 4), indicating no significant degradation of the catalysts during the experiment.
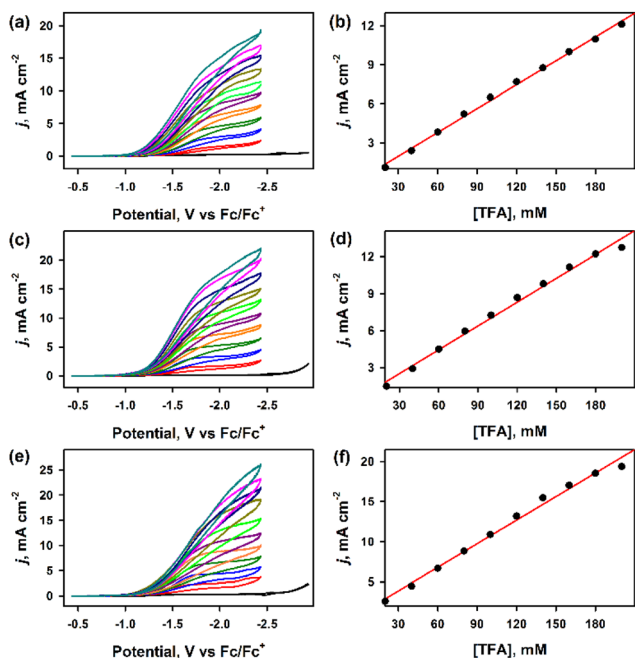
Fig. 3 CVs of 1 mM **1** (a), **2** (c), and **3** (e) in the presence of TFA (0–200 mM, the interval is 20 mM). Plots of catalytic peak current density (j) against the concentration of TFA for 1 mM **1** (b), **2** (d), and **3** (e) in CH_3CN.
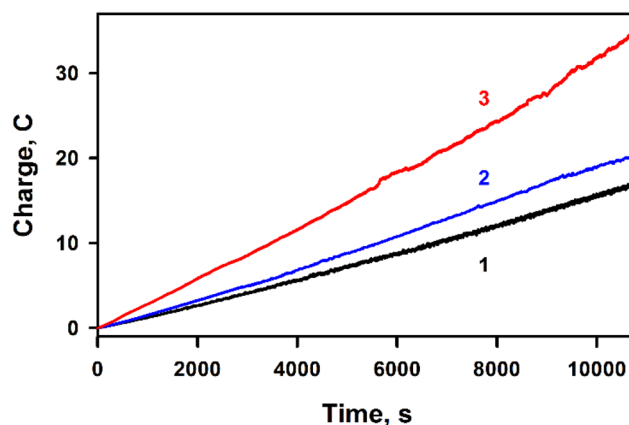
Fig. 4 Charge build-up *versus* time in extended CPE experiments of 1 mM **1–3** in the presence of 200 mM TFA in deaerated CH_3CN at −1.6 V for 3 h.

Based on the CV behavior of **1**–**3** in the presence or absence of TFA (Fig. 2 and 3), it is suggested that **1**–**3** catalyze proton reduction through an ECEC mechanism.[18] Upon addition of TFA, there is a significant positive shift in the onset potential for electrocatalytic hydrogen production compared to the Ni^{II}/Ni^{I} redox potential (Fig. 3a, c and e). This indicates the occurrence of the first EC process, leading to the formation of Ni^{III}–H species, followed by a one-electron reduction to give a Ni^{II}–H intermediate at a more positive potential than the Ni^{II}/Ni^{I} couple. It has been reported that Ni^{II}–H is more readily reduced compared to the corresponding Ni^{II} complex,[19] indicating that the ECEC pathway is more preferred. The electrochemical analysis method stands as a highly flexible technique for investigating homogeneous reactions. Notably, it provides valuable mechanistic insights into molecular catalysts for electrochemical HER, particularly through the analysis of cyclic voltammograms (CV) responses.[19] Based on the electrochemical studies and the previous reports,[20] a proposed catalytic cycle for the HER by neutral nickel(II) complexes bearing tetradentate NHC-amidate ligands is depicted in Fig. 5. The one-electron reduction of the starting Ni^{II} complex generates a Ni^{I} complex (pathway a), followed by protonation on the Ni atom to give a Ni^{III}–H intermediate (pathway b). Then, electron attachment to Ni^{III}–H generates the reduced Ni^{II}–H complex (pathway c), which releases H$_2$ upon protonation and regenerates the starting Ni^{II} complex (heterolytic pathway d). However, we cannot rule out the possibility of an alternative bimetallic pathway, where the reaction between two Ni^{III}–H complexes leads to the release of H$_2$ *via* reductive elimination (homolytic pathway e).

In summary, we have prepared three neutral nickel(II) complexes bearing tetradentate NHC-amidate ligands. The effects of the electronic properties of the ligand on the redox behavior and electrocatalytic activity for HER have been investigated. It was demonstrated that complex **3**, with the most positive potential, exhibits the highest electrocatalytic activity towards HER among the three complexes. Furthermore, an ECEC process was proposed for the HER based on the CV data of the nickel complexes after the addition of TFA. Therefore, this study lays the foundation for the intelligent design of efficient electrocatalytic molecular catalysts by controlling the electronic effects of the ligand. Our future study will concentrate on elucidating the nature of the active intermediate and the reaction mechanism through the synthesis, spectroscopic characterization, and kinetic studies of the implicated nickel-hydride species.

Data availability

The data supporting this article have been included as part of the ESI.†

Conflicts of interest

There are no conflicts to declare.

Acknowledgements

Fig. 5 Proposed mechanistic pathways for HER mediated by nickel complexes bearing tetradentate N-heterocyclic carbene amidate ligands.

References

1 Y. Li, X. Wei, L. Chen and J. Shi, *Angew. Chem., Int. Ed.*, 2021, **60**, 19550–19571.
2 D. Schilter, J. M. Camara, M. T. Huynh, S. Hammes-Schiffer and T. B. Rauchfuss, *Chem. Rev.*, 2016, **116**, 8693–8749.
3 J. R. McKone, S. C. Marinescu, B. S. Brunschwig, J. R. Winkler and H. B. Gray, *Chem. Sci.*, 2014, **5**, 865–878.
4 K. E. Dalle, J. Warnan, J. J. Leung, B. Reuillard, I. S. Karmel and E. Reisner, *Chem. Rev.*, 2019, **119**, 2752–2875.
5 H.-F. Wang, L. Chen, H. Pang, S. Kaskel and Q. Xu, *Chem. Soc. Rev.*, 2020, **49**, 1414–1448.
6 C. Elleouet, F. Y. Pétillon and P. Schollhammer, in *Non-Noble Metal Catalysis – Molecular Approaches and Reactions: Non-noble metal-based molecular catalysts for protons reduction*, ed. R. J. M. Klein Gebbink and M. E. Moret, Wiley-VCH, 2019, ch. 19, pp. 489–527.

7 B. M. Rosen, K. W. Quasdorf, D. A. Wilson, N. Zhang, A. M. Resmerita, N. K. Garg and V. Percec, *Chem. Rev.*, 2011, **111**, 1346–1416.

8 L. Gan, T. L. Groy, P. Tarakeshwar, S. K. S. Mazinani, J. Shearer, V. Mujica and A. K. Jones, *J. Am. Chem. Soc.*, 2015, **137**, 1109–1115.

9 (*a*) Z.-Y. Wu, T. Wang, Y.-S. Meng, Y. Rao, B.-W. Wang, J. Zheng, S. Gao and J.-L. Zhang, *Chem. Sci.*, 2017, **8**, 5953–5961; (*b*) M. L. Helm, M. P. Stewart, R. M. Bullock, M. R. DuBois and D. L. DuBois, *Science*, 2011, **333**, 863–866.

10 (*a*) S. Gaillard and J.-L. Renaud, *Dalton Trans.*, 2013, **42**, 7255–7270; (*b*) P. Bellotti, M. Koy, M. N. Hopkinson and F. Glorius, *Nat. Rev. Chem.*, 2021, **5**, 711–725.

11 A. John and P. Ghosh, *Dalton Trans.*, 2010, **39**, 7183–7206.

12 (*a*) S. Ray, J. Asthana, J. M. Tanski, M. M. Shaikh, D. Panda and P. Ghosh, *J. Organomet. Chem.*, 2009, **694**, 2328–2335; (*b*) J. Berding, T. F. van Dijkman, M. Lutz, A. L. Spek and E. Bouwman, *Dalton Trans.*, 2009, 6948–6955; (*c*) S. Luo, M. A. Siegler and E. Bouwman, *Eur. J. Inorg. Chem.*, 2016, **2016**, 4693–4700; (*d*) S. Luo, M. A. Siegler and E. Bouwman, *Eur. J. Inorg. Chem.*, 2019, **2019**, 617–627.

13 (*a*) K. V. Tan, J. L. Dutton, B. W. Skelton, D. J. D. Wilson and P. J. Barnard, *Organometallics*, 2013, **32**, 1913–1923; (*b*) M. C. Perry, X. Cui and K. Burgess, *Tetrahedron: Asymmetry*, 2002, **13**, 1969–1972.

14 L. Yang, D. R. Powell and R. P. Houser, *Dalton Trans.*, 2007, 955–964.

15 U. J. Kilgore, J. A. S. Roberts, D. H. Pool, A. M. Appel, M. P. Stewart, M. R. DuBois, W. G. Dougherty, W. S. Kassel, R. M. Bullock and D. L. DuBois, *J. Am. Chem. Soc.*, 2011, **133**, 5861–5872.

16 N. Wang, H. Lei, Z. Zhang, J. Li, W. Zhang and R. Cao, *Chem. Sci.*, 2019, **10**, 2308–2314.

17 (*a*) S. Roy, T.-A. D. Nguyen, L. Gan and A. K. Jones, *Dalton Trans.*, 2015, **44**, 14865–14876; (*b*) G. A. N. Felton, C. A. Mebi, B. J. Petro, A. K. Vannucci, D. H. Evans, R. S. Glass and D. L. Lichtenberger, *J. Organomet. Chem.*, 2009, **694**, 2681–2699.

18 V. Fourmond, P.-A. Jacques, M. Fontecave and V. Artero, *Inorg. Chem.*, 2010, **49**, 10338–10347.

19 (*a*) V. Artero and J. M. Saveant, *Energy Environ. Sci.*, 2014, **7**, 3808–3814; (*b*) D. J. Martin, B. D. McCarthy, E. S. Rountree and J. L. Dempsey, *Dalton Trans.*, 2016, **45**, 9970–9976.

20 (*a*) X. Guo, N. Wang, X. Li, Z. Zhang, J. Zhao, W. Ren, S. Ding, G. Xu, J. Li, U.-P. Apfel, W. Zhang and R. Cao, *Angew. Chem., Int. Ed.*, 2020, **59**, 8941–8946; (*b*) Y. Han, H. Fang, H. Jing, H. Sun, H. Lei, W. Lai and R. Cao, *Angew. Chem., Int. Ed.*, 2016, **55**, 5457–5462; (*c*) C. H. Lee, D. K. Dogutan and D. G. Nocera, *J. Am. Chem. Soc.*, 2011, **133**, 8775–8777; (*d*) J. L. Dempsey, J. R. Winkler and H. B. Gray, *J. Am. Chem. Soc.*, 2010, **132**, 16774–16776.